THE JOURNAL OF PHYSICAL CHEMISTRY C

Article

pubs.acs.org/JPCC

Defect Chemistry of Rutile TiO_2 from First Principles Calculations

Tor S. Bjørheim,[†] Akihide Kuwabara,[‡] and Truls Norby*,[†]

[†]Department of Chemistry, University of Oslo, Centre for Materials Science and Nanotechnology (SMN), Gaustadalléen 21, NO-0349 Oslo, Norway

[‡]Nanostructures Research Laboratory, Japan Fine Ceramics Center, 2-4-1 Mutsuno, Atsuta-ku, Nagoya, 456-8587 Japan

ABSTRACT: In the current contribution, we study the defect chemistry of bulk rutile TiO_2 through first principles defect calculations in combination with thermodynamic modeling. We apply three levels of theory, PBE, PBE+U, and the HSE hybrid functional. The defect calculations reveal that the included isolated defects, v_{Ti}^{q}, v_{O}^{q}, Ti_{i}^{q}, OH_{O}^{q}, and H_{O}^{q}, display shallow thermodynamic charge transition levels, whereas oxygen interstitials, O_{i}^{q}, display a deep (0/-2) transition level. The formation energies of the complexes between $v_{Ti}^{4/}$, $v_{O}^{\bullet\bullet}$, and $OH_{O}^{\bullet}$ are as low or even lower than those of the isolated defects, and all included complexes display exothermic binding enthalpies, indicating their possible presence under thermodynamic equilibrium. Through thermodynamic modeling, we show that the finite temperature defect structure of rutile TiO_2 largely is dominated by $v_{Ti}^{4/}$, $OH_{O}^{\bullet}$, and their mutual complexes under wet oxidizing conditions and lower temperatures and by $v_{Ti}^{4/}$, $v_{O}^{\bullet\bullet}$, and their complexes at higher temperatures. Hence, we indicate that TiO_2 cooled from high temperatures or grown at low temperatures will display defect structures very different from previously known, which together with previous results for defects in surfaces gives a new basis for understanding for instance photocatalytic properties of TiO_2.

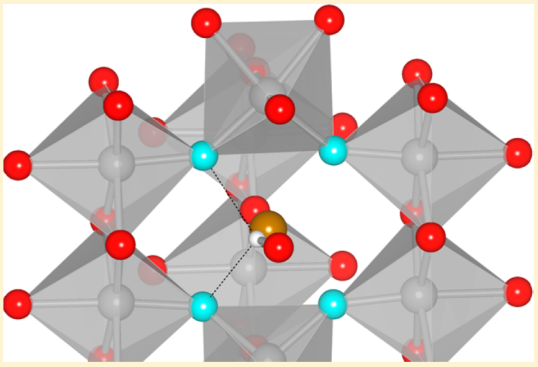

1. INTRODUCTION

Rutile TiO_2, a simple binary wide-gap oxide semiconductor, has in the recent years attracted much attention due to its numerous applications mainly connected with its optical and photocatalytic properties. Although the material has been studied extensively since the discovery of its photocatalytic properties in the 1970s,[1] many aspects of its properties and mechanisms of operation remain unknown.

Experimentally, as-prepared rutile TiO_2 is known to be an n-type semiconductor under reducing conditions and higher temperatures.[2] This is usually explained by a defect situation where oxygen vacancies and electrons dominate

$$O_O^{\times} = v_O^{\bullet\bullet} + 2e^{/} + \frac{1}{2}O_2(g) \quad (1)$$

resulting in defect concentrations and an n-type conductivity proportional to $p_{O_2}^{-1/6}$. Under more oxidizing conditions, the bulk conductivity is shown to approach a $p_{O_2}^{-1/4}$ dependency, explained by a defect regime governed by ionic defects with electronic defects being in minority concentration-wise. Although traditionally neglected in the evaluation of defect equilibria in TiO_2,[2,3] hydrogen in the form of protonic defects, $OH_O^{\bullet}$, plays a major role in the electrical properties and defect chemistry of rutile TiO_2.[4−14] Protons have been shown to incorporate from water vapor containing atmospheres according to

$$H_2O(g) + O_O^{\times} + v_O^{\bullet\bullet} = 2OH_O^{\bullet} \quad (2)$$

i.e., by replacement of oxygen vacancies as the majority positive charge compensating defect, for which a hydration enthalpy of −1.35 eV (for eq 2) was deduced from conductivity measurements.[10] Under oxidizing conditions, the increasing concentration of protons with increasing p_{H_2O} was found to reduce the minority concentration of electron holes and thus the p-type conductivity, and to increase the minority concentration of electrons and thus the n-type conductivity under reducing conditions.

In undoped TiO_2, one may foresee hydrogen to be incorporated by creation of charge compensating electrons under very reducing conditions or Ti vacancies under oxidizing

$$H_2(g) + 2O_O^{\times} = 2OH_O^{\bullet} + 2e^{/} \quad (3)$$

$$2H_2O(g) + 2O_O^{\times} = 4OH_O^{\bullet} + v_{Ti}^{4/} \quad (4)$$

At lower temperatures, and in the case of a defect situation given by eq 4, one may also foresee association of $OH_O^{\bullet}$ with the highly charged $v_{Ti}^{4/}$ in the form of $(v_{Ti}nOH_O)^{q}$. In our previous theoretical work,[9] we showed that these complexes were stable in terms of exothermic binding enthalpies. Such complexes are well-known in for instance MnO_2 where they are termed Ruetschi defects,[15] have been described in anatase TiO_2,[16] and

Received: April 30, 2012
Revised: February 12, 2013
Published: February 13, 2013

have been shown to exhibit exothermic binding enthalpies in other semiconducting oxides such as In_2O_3, Ga_2O_3 and SnO_2.[17]

Regarding the defect chemistry of TiO_2, an often encountered discussion is whether various defects result in polaronic trapping of electrons and holes (cf. refs 4 and 18−32). Photoelectron spectroscopy on defective rutile TiO_2 single crystals has indicated an in-gap defect state 0.9 eV below the conduction band (CB),[18−20] which from EPR measurements has been suggested to be due to polaronic trapping of electrons as localized $Ti_{Ti}^{/}$ defects.[21,22] A large number of DFT studies have indicated that almost all donor defects with excess electrons display such in-gap defect states in rutile TiO_2.[25−35] Similarly, polaronic trapping of electron holes may occur at oxide ions (in the form of $O_O^{\bullet}$ defects) neighboring acceptor defects. Morgan and Watson[27] for instance showed this to be the case of Ti vacancies in anatase, for which they reported trapping of up to four electron holes in the form of localized hole polarons on the O ions neighboring the Ti vacancy. Interestingly, Deák et al.[36] recently reported, using the hybrid functional HSE06, that anatase tends to localize hole polarons for acceptor defects to a larger extent than rutile, while rutile tends to localize electron polarons for donor defects to a larger extent than anatase. The actual depth or stability of these defect states, and position of the $Ti_{Ti}^{/}/O_O^{\bullet}$ with respect to the ionic defects greatly depends on the adopted computational methodology; while LDA/PBE (cf. refs 9,32,37) only yields delocalized solutions, both DFT+U and hybrid functional calculations have been shown to yield the localized ground states (cf. refs 13−16,21−25). Peng reported shallow thermodynamic charge transition levels for v_O^q, Ti_i^q, and v_{Ti}^q using PBE, while He et al.[38] and Li et al.[39] on the other hand obtained in-gap transition levels for all included defects using PBE. Similarly, several studies applying the +U functional have reported in-gap transition levels of v_O^q and Ti_i^q.[40,41] Recently, Janotti et al.[31] showed through hybrid functional (HSE) calculations on rutile that, despite the creation of in-gap states in the case of $v_O^{\times}$ (or a $v_O^{\bullet\bullet}$ and two $Ti_{Ti}^{/}$ bound in a complex), the isolated $v_O^{\bullet\bullet}$ has a lower formation energy under all conditions, and oxygen vacancies are in fact shallow donors, with a modest binding energy to $Ti_{Ti}^{/}$.

In this work we aim at a detailed first principles defect chemical study of rutile TiO_2 using three levels of theory (PBE, PBE+U and the hybrid functional HSE) to elaborate on the electronic properties and stability of common point defects and their mutual complexes, and their impact on the high temperature defect chemistry of rutile. Although similar evaluations have been reported by for instance Peng[37] and He et al.,[38] previous studies are typically based on LDA/PBE calculations and neglect the effect of protons and complex formation on the defect chemistry. Here we evaluate finite temperature and partial pressure defect formation energies, and the resulting concentrations, through combination of DFT and temperature dependent atomic chemical potentials, thus simplifying the defect formation entropies to those associated with exchange of atomic species. Finally, we apply the concept of electroneutrality to determine the equilibrium Fermi level and thus all defect concentrations under thermal equilibrium conditions.

2. COMPUTATIONAL DETAILS

All calculations are performed within the density functional theory (DFT) formalism as implemented in VASP.[42,43] We employ the generalized gradient approximation functional due to Perdew, Burke, and Ernzerhof (GGA-PBE)[44] and the hybrid functional due to Heyd, Scuseria, and Ernzerhof with a screening parameter of 0.2 (HSE06).[45,46] For the hybrid calculations, we intermix 20% HF exchange (compared to the default value of 25%), referred to as "HSE" throughout this manuscript.[31] Further, we utilize the on-site +U extension (PBE+U) with U = 4.2 eV for the Ti 3d states. Although the optimal U value depends on the choice of functional, this value has previously been adopted in several similar studies[25,26] and is close the value proposed by Bocquet et al.[47] from 2p core-level X-ray photoemission spectroscopy (XPS). All calculations were performed using the projector augmented-wave (PAW) method[48] and a constant energy cutoff of 500 eV for the plane-waves.

With PBE and +U, we employ supercells from 72 to 576 atoms, while the HSE calculations were performed using a 72 atoms supercell. Defect formation energies from the HSE calculations are extrapolated to those of a supercell containing 576 atoms according to the supercell size dependence of the formation energies in the PBE and +U calculations. Calculations are performed with a 2×2×2 **k**-mesh for the 72 atoms supercells. For larger cells, the **k**-mesh was reduced accordingly.

All calculations are performed by allowing relaxation of all ionic positions with residual forces convergence criterion of 0.02 eV/Å (0.05 eV/Å for HSE) and energy convergence criterion of 10^{-6} eV for electronic self-consistency. In all defect calculations, the lattice shape and volume is fixed to that of the pristine supercell. The vibrational modes of selected defects are obtained within the harmonic approximation from finite displacements of 0.015 Å in all directions, by allowing displacement of the 12 nearest oxide ions. The phonon calculations are performed using PBE and accurately optimized structures, for which the convergence criteria were decreased to 10^{-4} eV/Å and 10^{-8} eV.

Table 1 lists the lattice constants and formation energy of rutile TiO_2 calculated using the various functionals. As expected, both PBE and +U overestimate the lattice constants slightly, due to the underbinding nature inherent within GGA, whereas those calculated using HSE are closer to the experimentally determined parameters. More severely, both PBE and +U, heavily underestimates the band gap, whereas the HSE gap closely matches the experimental one. Finally, the formation energy of the oxide is somewhat overestimated within PBE, whereas those calculated with +U and HSE are closer to the experimental value. As inclusion of the Coulomb term on the Ti 3d states does not affect the total energy of the O_2 molecule, the difference between PBE and +U is here a result of the effect of the additional Coulomb term on the Ti 3d orbitals in TiO_2 and α-Ti.

Table 1. Lattice Parameters, Band Gap, and Formation Enthalpy of Rutile TiO_2 Calculated with the Different Functionals Implemented in This Work

	PBE	+U	HSE	exp.
a/Å	4.6507	4.6809	4.6029	4.5937[49]
c/Å	2.9690	3.0279	2.9529	2.9587[49]
ΔH^f/eV	−9.06	−9.71	−9.64	−9.79[50]
E_g/eV	1.77	2.21	3.01	3.035[51]

3. THEORETICAL FORMALISM

The defect formation energies are obtained through

$$\Delta G_{\mathrm{defect}}^{\mathrm{f}} = E_{\mathrm{defect}}^{\mathrm{tot}} - E_{\mathrm{bulk}}^{\mathrm{tot}} + \sum_{1}^{i} \Delta n_i \mu_i + q(\mu_e + \Delta) \quad (5)$$

dx.doi.org/10.1021/jp304146e | J. Phys. Chem. C 2013, 117, 5919−5930

where μ_i are the chemical potentials of the involved atomic species and μ_e is the Fermi level. Δn_i is the change in the number of atom i between the perfect and defective cell. In the case of a vacancy and an interstitial defect, Δn_i is 1 and −1, respectively. Δ aligns the core levels of the defective and pristine systems in order to account for the artificial interactions caused by the jellium background in the charged, defective systems.[52] The 0 K formation energies are evaluated under wet, oxidizing conditions with the chemical potentials fixed to

$$\mu_{Ti} = \mu^{\circ}_{TiO_2} - \mu^{\circ}_{O_2} \quad (6)$$

$$\mu_O = \frac{1}{2}\mu^{\circ}_{O_2} \quad (7)$$

$$\mu_H = \frac{1}{2}\left(\mu^{\circ}_{H_2O} - \frac{1}{2}\mu^{\circ}_{O_2}\right) \quad (8)$$

where $\mu^{\circ}_{TiO_2}$, $\mu^{\circ}_{O_2}$, and $\mu^{\circ}_{H_2O}$ are set to the total energies of the pure phases as obtained from DFT.

For finite temperature and partial pressures, the temperature and partial pressure dependencies of all atomic chemical potentials in eq 5 are included by

$$\mu_i(T, p_i) = \mu_i^{\circ} + H_i(T, p^{\circ}) - TS_i(T, p^{\circ}) + k_b T \ln(p_i/p^{\circ}) \quad (9)$$

where the second and third terms are taken as tabulated values.[50] This procedure simplifies the defect formation entropies to those associated with exchange of atomic species, whereas contributions from vibrational entropy changes within the crystal itself upon defect formation are neglected. This approach has been justified by for instance Björketun et al.[53] and is not expected to alter major defect trends but might affect the temperature at which a given defect structure will become dominating somewhat. To avoid the large uncertainty arising from overbinding of the O_2 molecule in evaluation of finite temperature formation energies, we obtain μ_O by assuming the equilibrium gas mixture $H_2O(g) + H_2(g)$ in which μ_O is given by $\mu_O(T, p_{O_2}) = \mu_{H_2O}(T, p_{H_2O}) - 2\,\mu_H(T, p_{H_2})$.

Finite temperature and partial pressure defect concentrations are obtained through

$$\frac{[\text{defect } i]}{c_{s,0}} = N_{\text{config}} \exp\left(-\frac{\Delta G^{f}_{\text{defect}}}{k_b T}\right) \quad (10)$$

where $c_{s,0}$ is the concentration of regular particles on which the defect may form (for instance concentration of $O^{\times}_O$ or $Ti^{\times}_{Ti}$) and N_{config} is the number of configurations the defect may attain at each site, respectively. Upon defect formation, the concentration of $O^{\times}_O$ or $Ti^{\times}_{Ti}$ (i.e., $c_{s,0}$) must fulfill

$$\begin{aligned}&[H^q_O] + [OH^q_O] + [v^q_O] + n[(v_{Ti}nOH_O)^q] \\ &\quad + 2[(v_{Ti}v_OOH_O)^q] + 3[(v_{Ti}v_O2OH_O)^q] + [(v_{Ti}v_O)^q] \\ &\quad + 2[(v_{Ti}2v_O)^q] + [(O_2)^q_O] + [O^{\times}_O] = 2\end{aligned} \quad (11)$$

$$\begin{aligned}&[v^q_{Ti}] + n[(v_{Ti}nOH_O)^q] + [(v_{Ti}v_OOH_O)^q] \\ &\quad + [(v_{Ti}v_O2OH_O)^q] + [(v_{Ti}v_O)^q] + [(v_{Ti}2v_O)^q] \\ &\quad + [Ti^{\times}_{Ti}] = 1\end{aligned} \quad (12)$$

The equilibrium Fermi level is determined by applying the concept of electroneutrality

$$\sum_{i=0}^{n} q[\text{defect } i] + p - n = 0 \quad (13)$$

where p and n (electron hole/electron concentrations) are obtained from the calculated density of states, $D(\epsilon_i)$, and the Fermi distribution, $f_e(\epsilon_i)$

$$n = \int_{CBM}^{\infty} D(\epsilon_i) f_e(\epsilon_i)\, d\epsilon_i \cong \sum_{i=CBM}^{\infty} D(\epsilon_i) \exp\left(-\frac{\epsilon_i - \mu_e}{k_b T}\right) \quad (14)$$

$$p = \int_{-\infty}^{VBM} D(\epsilon_i) f_h(\epsilon_i)\, d\epsilon_i \cong \sum_{i=-\infty}^{VBM} D(\epsilon_i) \exp\left(-\frac{\mu_e - \epsilon_i}{k_b T}\right) \quad (15)$$

where μ_e is the Fermi level. The Fermi level and the individual defect concentrations may thus be obtained by solving eq 13 for each atmospheric condition.

4. DEFECTS IN RUTILE

To evaluate the defect chemistry of rutile TiO_2, we have considered the native point defects:

- Titanium vacancies, v^q_{Ti} with $q \in [-4, 0]$
- Oxygen vacancies, v^q_O with $q \in [0, +2]$
- Titanium interstitials, Ti^q_i with $q \in [0, +4]$
- Oxygen interstitials, O^q_i with $q \in [-2, 0]$

the hydrogen related extrinsic defects:

- Interstitial, H^q_i (or OH^q_O) with $q \in [-1, +1]$
- Substitutional H, H^q_O with $q \in [0, +1]$

and the association complexes;

- $(v_{Ti}nOH_O)^q$ with $n \in [1, 4]$
- $(v_{Ti}v_OnOH_O)^q$ with $n \in [1, 2]$
- $(v_{Ti}nv_O)^q$ with $n \in [1, 2]$

4.1. Isolated Point Defects. *Site Preference.* Whereas there is only a single site on which v^q_{Ti}, v^q_O, and H^q_O may form, the interstitial defects OH^q_O, Ti^q_i, and O^q_i may take on several positions in the rutile structure. Interstitial H has been shown to locate in positions close to the oxide ions (in the form of OH^q_O) with the O−H axis oriented in the a-b plane toward the open 'channels' along the c-axis.[9,11] The Ti^q_i defect may in principle occupy the empty tetrahedral (4-fold coordinated to O) or octahedral sites (6-fold coordinated to O). However, we find the defect to be ∼3 eV more stable in the octahedral sites, and we will only consider this position in the following discussion. Interstitial oxide ions, O^q_i, may also occupy octahedral and tetrahedral sites. However, as shown by Kamisaka and Yamashita,[54] the most stable configurations are in the form of a peroxide defect, $(O_2)^q_O$. The interstitial O bonds to a lattice oxygen and displaces it slightly from its lattice position, thus rendering two Ti ions 7-fold coordinated. The O−O bond length depends on the charge of the defect, and was within the HSE functional found to be 1.42, 1.86, and 2.11 Å for the three charge states 0, −1, and −2, respectively.

Defects and Polaron Trapping. With PBE, no in-gap defect states were observed for any of the donor defects Ti^q_i, v^q_O, OH^q_O or H^q_O. On the other hand, both +U and HSE gave localized solutions and in-gap states upon formation of the donor defects with excess electrons as shown by the DOS of OH^q_O ($q = 0$ and 1) in Figure 1 (HSE), in accordance with literature.[18−32] Whereas OH^q_O ($q = 0$) yielded a single state ∼0.8 eV below the conduction band (CB), the extra electron of OH^q_O ($q = -1$) resulted in a

dx.doi.org/10.1021/jp304146e | J. Phys. Chem. C 2013, 117, 5919−5930

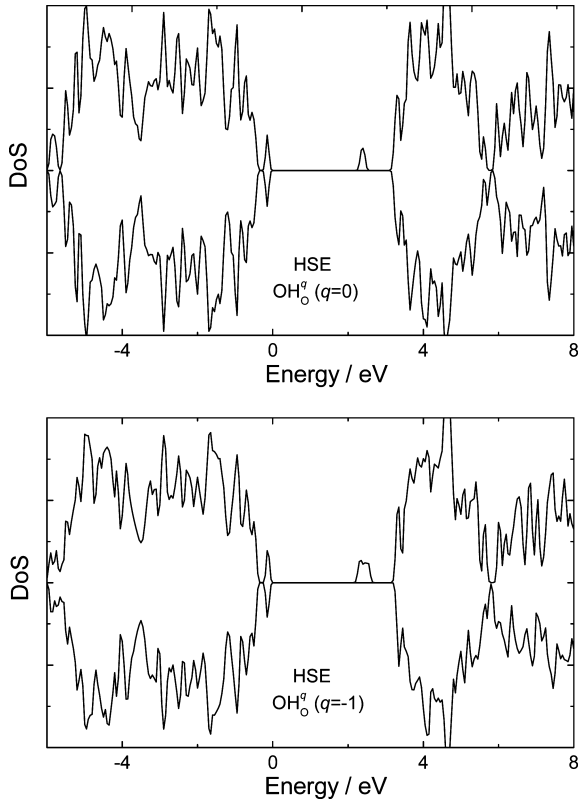

Figure 1. Calculated density of states for OH_O^q ($q = 0$ and -1) using the HSE functional.

second, spin-polarized state slightly closer to the conduction band. With +U the states appear slightly deeper, 1.1 to 1.3 eV below CB for Ti_i^q ($q = +3$), OH_O^q ($q = 0$), OH_O^q ($q = 0$), and v_O^q ($q = 0$ and +1), in agreement with for instance Morgan and Watson using the same +U parameter.[28] The partial charge densities associated with these defect states (Figure 2) show that the defect state of Ti_i^q ($q = +3$) is associated with the defect itself (i.e., a $Ti_i^{3\bullet}$ defect), while that of OH_O^q ($q = 0$) is associated with a bulk and the nearest neighbor Ti ions. For OH_O^q ($q = 0$), Deák et al.[36] showed that this configuration is a consequence of the small supercell, and the defect is thus better described as a complex of the ionized defect and an electron polaron, $(OH_OTi_{Ti})^\times$. Similar localized solutions were obtained also for OH_O^q ($q = -1$) and H_O^q ($q = 0$). For v_O^q ($q = 0$ and +1) the defect levels were associated with only two of the nearest neighbor Ti ions, in agreement with the HSE (20% HF) calculations of Janotti et al.,[31] and the defects are better represented as the complexes $(v_O2Ti_{Ti})^\times$ and $(v_OTi_{Ti})^/$.

The only donor defect which may display multiple charge states is thus the Ti interstitial (i.e., $Ti_i^{4\bullet}/Ti_i^{3\bullet}$), while the remaining defects may form association complexes with the $Ti_{Ti}^/$ defects. The only partly associated ground states obtained for $(OH_OTi_{Ti})^\times$ and $(H_OTi_{Ti})^\times$ in HSE indicate a modest binding enthalpy of the complexes which is counteracted by the small supercell used in the HSE calculations. Similarly, the associated ground state configurations of $(v_O2Ti_{Ti})^\times$ and $(v_OTi_{Ti})^/$ indicate a somewhat stronger association of these complexes. However, we were unable to quantify the binding enthalpies of the complexes since all attempts to obtain a localized ground state of $Ti_{Ti}^/$ in an otherwise defect free supercell resulted in delocalized solutions.

It is well-known that the degree of localization varies with, for instance, the choice of the Hubbard-U parameter.[30] In addition, it has also been argued that varying the amount of HF exchange in HSE to match the experimental and theoretical band gap could result in wrongfully predicted defect properties[36] and that a reduced HF fraction would favor delocalized solutions. In our calculations, the optical transition level of, for instance, OH_O^q ($q = 0$) using 20% HF was found to be 0.60 eV below CB while 25% HF yielded a slightly deeper transition level at 0.82 eV below CB, in agreement with Deák et al.[36] v_O^q ($q = 0$) displays two ionization levels, $0 \rightarrow +1$ and $+1 \rightarrow +2$, for which we found optical ionization levels of 0.39/0.91 eV, and 0.60/1.15 eV with 20 and 25% HF, respectively. Hence, both functionals reproduce the localized ground states of the donor defects, as indicated experimentally, but HSE with 25% HF yields optical transition levels slightly closer to the experimental defect level at 0.9 eV below CB as indicated by ultraviolet photoelectron spectroscopy (UPS).[18]

For v_{Ti}^q we obtained delocalized hole states for the defect in all possible charge states with the three functionals, in line with the HSE06 calculations by Deák et al.[36] on substitutional acceptors in rutile TiO_2. Hence, the behavior of the Ti vacancy is fundamentally different in anatase and rutile; while it is a shallow acceptor in rutile, it may lead to polaronic trapping of holes in anatase and thus take on multiple charge states.[27]

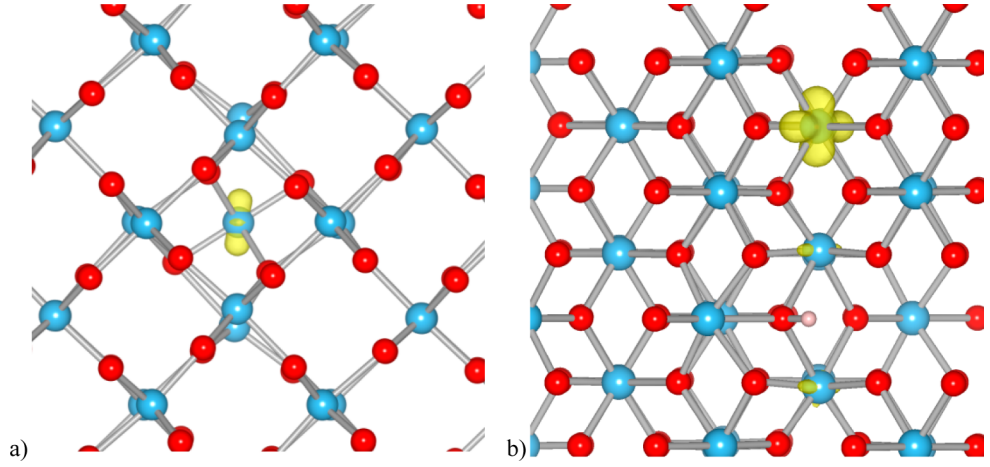

Figure 2. Partial charge densities of the in-gap defect state for (a) $Ti_i^{3\bullet}$ and (b) OH_O^q ($q = 0$) as obtained with the HSE functional (20% HF).

dx.doi.org/10.1021/jp304146e | J. Phys. Chem. C 2013, 117, 5919−5930

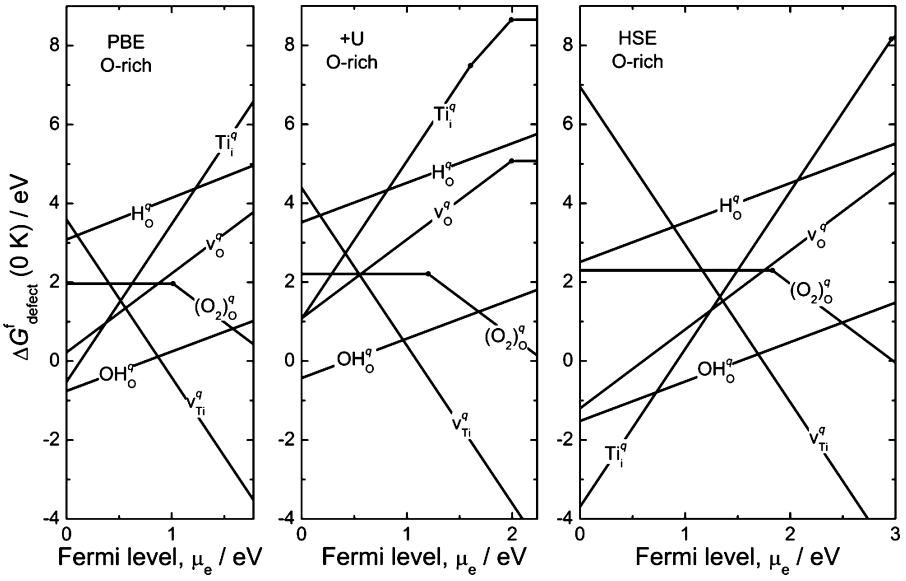

Figure 3. Formation energies of various isolated point defects as a function of the Fermi level under oxygen-rich conditions at 0 K as obtained using the different functionals.

For the $(O_2)_O^q$ defect, Kamisaka and Yamashita argued (using GGA+U) that addition of 1 or 2 electrons to $(O_2)_O^\times$ results in occupation of a antibonding state, thus explaining the gradual increase in the O−O bond length with increasing number of electrons. For anatase, they showed that this occupied state appeared within the band gap for both the −1 and −2 charge states. Also in our HSE calculations, we find that the −1 and −2 charge states result in occupation of a state with 2p character, associated with both oxide ions. This occupied state is found at the very top of the valence band, contrary to the results for anatase by Kamisaka and Yamashita.[54]

Thermodynamic Stability. Figure 3 displays the formation energies (according to eq 5) of all isolated point defects in their possible charge states under oxygen-rich conditions at 0 K, as emerging from the PBE, +U and HSE functionals (with no corrections due to the underestimated band gap in the case of PBE and +U). We note that our PBE formation energies are comparable to the LDA results of Peng,[37] while our HSE formation energy of $v_O^{\bullet\bullet}$ is comparable to that reported by Janotti et al.[31]

The thermodynamic transition levels of v_{Ti}^q falls below the valence band maximum with all functionals, as expected from the delocalized hole states of the un-ionized defect. v_{Ti}^q will therefore be present as $v_{Ti}^{4/}$. Further, the (0/−2) transition level of $(O_2)_O^q$ falls within the gap with transition levels at 1.0, 1.2, and 1.9 eV above the valence band with PBE, +U and HSE, respectively. In comparison, Lee et al. reported a (0/−2) level at 1.2 eV using the screened exchange hybrid functional (sX).[55] Further, the thermodynamic transition levels of the donor defects OH_O^q, H_O^q, Ti_i^q and v_O^q all fall at or slightly above the CB with PBE and HSE. With the +U functional, the (+4/+3) and (+3/0) transition levels of Ti_i^q and the (+2/0) level of v_O^q appear within the theoretical band gap, as also reported by for instance Park et al.,[41] whereas those of OH_O^q and H_O^q still appear above the CBM. However, only the (+4/+3) level of Ti_i^q reflects reduction of the actual defect from $Ti_i^{4\bullet}$ to $Ti_i^{3\bullet}$, while the (+3/0) level reflects $Ti_i^{3\bullet}$ to $(Ti_i 3Ti_{Ti})^\times$. The in-gap transition levels indicate that the additional Coulomb term in the +U functional increases the stability of $Ti_{Ti}^{/}$ (and also $Ti_i^{3\bullet}$) and thus the binding enthalpies of its complexes with the donor defects. Nevertheless, from the HSE results, we conclude that all included donors display shallow thermodynamic transition levels, in contrast to the deep optical transition levels of the donor defects described in the preceding section. This difference may be attributed to favorable relaxations of the ionized donor defects compared the localized solutions of the un-ionized defects, as also shown by Janotti et al.[31] for v_O^q. Hence, the defects themselves will exist in the fully ionized charge states $OH_O^\bullet$, $H_O^\bullet$, $Ti_i^{4\bullet}$, and $v_O^{\bullet\bullet}$ under equilibrium conditions, while the defect-polaron complexes may be present as minority defects in n-type TiO_2. We thus neglect such complexes in the further evaluation of the defect properties of rutile TiO_2. We note that application of 25% HF exchange (which yields a band gap of 3.4 eV) would stabilize these defect-polaron complexes and pull the thermodynamic transition levels of the donor defects slightly below the conduction band. In comparison, Janotti et al.[31] also reported a shallow thermodynamic (+2/0) transition level for oxygen vacancies with HSE and 20% HF. On the other hand, Lee et al.[55] recently reported a (+2/0) level for v_O^q at 2.3 eV and a (+4/0) level for Ti_i^q at 2.85 eV above the valence band based on the screened exchange functional. This discrepancy could be due to differences in the applied pseudopotentials, or in the treatment of the exchange screening in the HSE and sX functionals. However, we rationalize our choice of functional by that our calculated optical transition levels are comparable with those from UPS. Further, an accurate band gap is essential to predict correct thermal equilibrium Fermi levels and thus concentrations of electronic charge carriers. Nevertheless, a detailed study of the electronic structure of these defect-polaron complexes using for instance the GW approach is called for.

Widening of the band gap from PBE to +U to HSE obviously has a drastic effect on the defect formation energies; the formation energies of all donor defects at the VBM are lower with HSE than with PBE/+U, whereas that of $v_{Ti}^{4/}$ is higher in HSE than in PBE/+U. The formation energy of neutral $(O_2)_O^\times$ is on the other hand comparable with the three functionals. This indicates that the formation energies mostly are affected by the position of the band edges, and thus the reference level of μ_e. In the case of PBE vs HSE, Janotti et al.[31] reported a downward shift of the valence band by 0.6 eV and an upward shift by 0.7 eV of the

dx.doi.org/10.1021/jp304146e | J. Phys. Chem. C 2013, 117, 5919−5930

conduction band states. We note that the HSE formation energies at $\mu_e = 0.6$ eV are comparable to the PBE results at $\mu_e = 0.0$ eV. To exclude the effect of changes in μ_e, one may compare defect reactions that are independent of the Fermi level, for instance the hydration equilibrium, and Frenkel and Schottky formation

$$H_2O + v_O^{\bullet\bullet} + O_O^{\times} = 2OH_O^{\bullet} \quad (16)$$

$$Ti_{Ti}^{\times} = Ti_i^{4\bullet} + v_{Ti}^{4/} \quad (17)$$

$$\text{null} = v_{Ti}^{4/} + 2v_O^{\bullet\bullet} \quad (18)$$

for which the enthalpies are given by

$$\Delta_{Hydr}H = 2\Delta H^f_{OH_O^{\bullet}} - \Delta H^f_{v_O^{\bullet\bullet}} \quad (19)$$

$$\Delta_{Frenkel}H = \Delta H^f_{Ti_i^{4\bullet}} + \Delta H^f_{v_{Ti}^{4/}} \quad (20)$$

$$\Delta_{Schottky}H = \Delta H^f_{v_{Ti}^{4/}} + 2\Delta H^f_{v_O^{\bullet\bullet}} \quad (21)$$

The obtained hydration enthalpies (see Table 2) are exothermic and comparable within the three functionals. The values are also comparable to what we reported in our previous study[9] (PBE result) and to the experimentally determined enthalpy.[10] In the case of Frenkel and Schottky formation, PBE and HSE again give nearly identical values, whereas the +U values are significantly higher. Hence, the major change in the formation energies between PBE and HSE is due to displacement of the band edges, whereas structural relaxations and changes in the atomic chemical potentials only have a minor effect on the defect properties. With +U, however, the reaction occurring in the oxygen lattice is well described while the large discrepancy in the Frenkel enthalpy indicates a compositional dependence of the on-site Coulomb repulsion in the +U approach.

Table 2. Hydration, Frenkel, and Schottky Formation Enthalpies As Obtained with the Three Employed Functionals

	PBE	+U	HSE
hydration/eV	−1.74	−1.86	−1.84
Frenkel/eV	3.07	5.46	3.19
Schottky/eV	4.03	6.55	4.55

4.2. Defect Complexes. *Complex Pair Orientations.* To obtain an accurate description of the defect complexes outlined in section 4, we have initially studied their configurational degeneracy. Ti is 6 fold (octahedrally) coordinated in the rutile structure, with 4 equidistant O ions (denoted O_a) forming the basal plane of the octahedron, and 2 equidistant O ions (denoted O_b) on each side of the basal plane. There are two equivalent proton sites per O ion in the rutile structure[9,11] and thus 12 proton sites on the O ions surrounding a given Ti ion (see Figure 4), resulting in a large number of possible configurations of the $(v_{Ti}nOH_O)^q$ complexes (Ruetschi type defects).

For $(v_{Ti}OH_O)^q$, the two most stable configurations are those where the proton is slightly tilted from the H_a and H_b sites toward the vacancy (see Figure 5a and b). The configuration with H_a (Figure 5a) is 0.15 eV more stable than H_b (Figure 5b) and there are thus 8 possible pair orientations of such a complex per Ti ion. Similarly, for $(v_{Ti}2OH_O)^q$, the most stable configurations are those with both protons located in the H_a positions, which are 0.27 eV more stable than configurations with both protons originally in the H_b sites and 0.13 eV more stable than the complex with one H_a and one H_b. Assuming that only the low energy configurations are significantly populated at lower temperatures, there are thus 22 possible pair orientations of this complex. Increasing the number of protons in the complex alters the relative stability of the H_a and H_b sites, and the most stable configurations of the $(v_{Ti}4OH_O)^q$ are those with two H_a and two H_b (with the two H_a and H_b in an antiparallel arrangement as depicted in Figure 5c,d). The two configurations are within 30 meV of each other and will thus both be equally populated even at room temperature. With the restriction of 2 antiparallel H_a and 2 antiparallel H_b, there are 8 possible pair orientations for this complex per Ti ion.

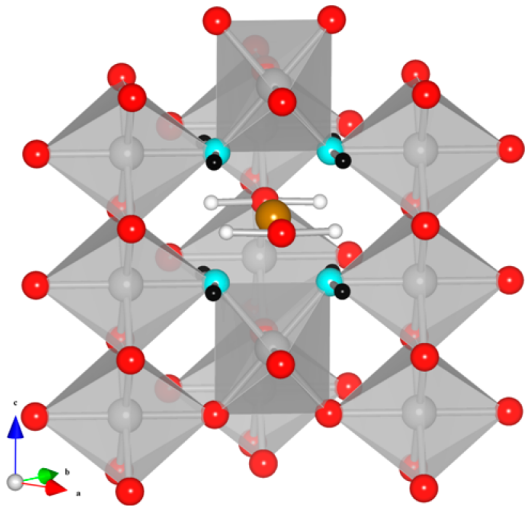

Figure 4. Oxygen and proton sites surrounding a Ti vacancy (brown sphere). The light blue spheres indicate the 4 O_a ions forming the basal plane of the TiO_6 octahedron whereas the small black spheres show the proton sites associated with these O ions (denoted H_a) in the text. Similarly, the small white spheres indicate the 4 proton sites associated with the 2 O_b ions on each side of the basal plane of the TiO_6 octahedron (denoted H_b).

In $(v_{Ti}v_O)^q$ and $(v_{Ti}2v_O)^q$, the oxygen vacancies may form on the two different O ions surrounding a given Ti ion. For $(v_{Ti}v_O)^q$, the complex with the O vacancy on an O_a site is 0.46 eV lower than that with the vacancy on the O_b site, and there are thus 4 possible configurations of the complex per Ti ion. Similarly, the most stable configuration of $(v_{Ti}2v_O)^q$ are those with one oxygen vacancy in O_a and one on O_b and there are thus 8 configurations for the complex per Ti ion.

Thermodynamic Stability. Figure 6 presents the formation energies of all included association complexes with HSE in the O-rich limit. As for the isolated Ti vacancy, all its complexes also displayed delocalized hole states for the un-ionized defects, yielding shallow thermodynamic charge transition levels. Hence, their effective charge states are fixed to those determined by the charge states of the isolated point defects (see list in Table 3). We further note that many of the complexes have as low or lower formation energies than the isolated point defects, indicating that they should be accounted for when considering the defect chemistry of rutile TiO_2.

The thermodynamic stability of such complexes are, in addition to their formation energies, described by their binding enthalpies (here defined as exothermic for a stable complex)

$$\Delta H^A_{complex} = \Delta H^f_{complex} - \sum \Delta H^f_{isolated\ defects} \quad (22)$$

dx.doi.org/10.1021/jp304146e | J. Phys. Chem. C 2013, 117, 5919−5930

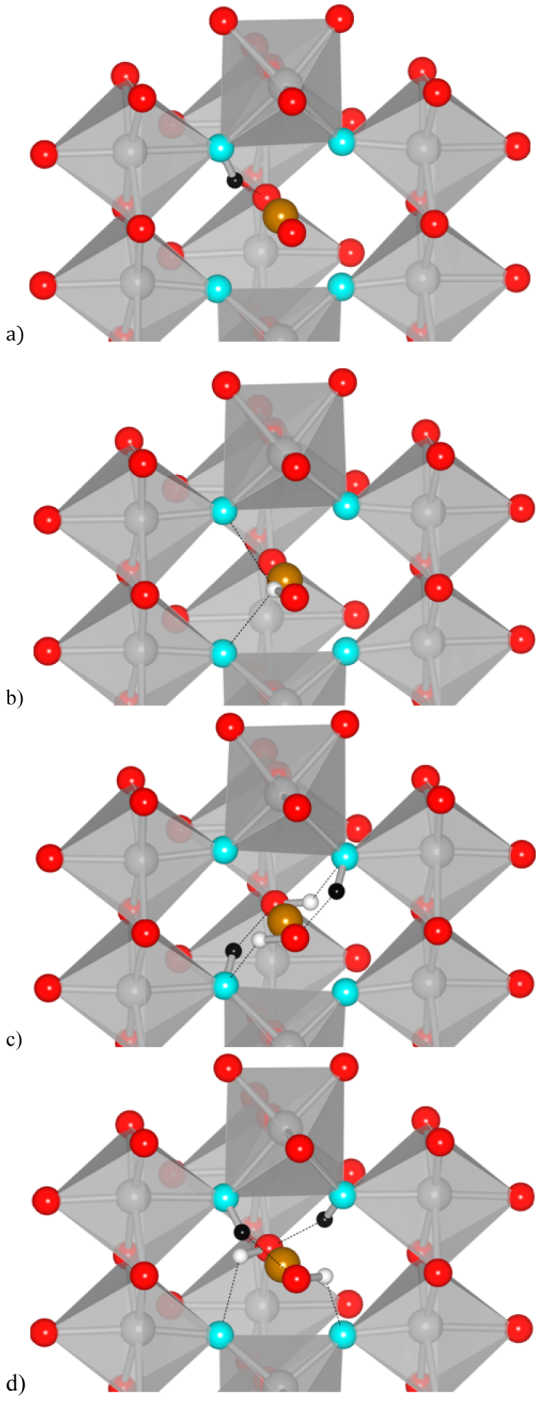

Figure 5. Low energy configurations of the $(v_{Ti}OH_O)^{3/}$ complex with the hydrogen in H_a (a) and H_b (b) and the $(v_{Ti}4OH_O)^{\times}$ with two antiparallell H_a (c) and two antiparallel H_b (d).

Table 3 displays the binding enthalpies of all included complexes calculated with the three functionals. All binding enthalpies are negative, indicating that the isolated point defects will tend to associate. Further, both PBE and HSE again give binding enthalpies in fair agreement, whereas the +U results deviate significantly, thus elaborating the observations in the preceding section. The minor differences between the PBE and HSE results may be attributed to different structural relaxations of the complexes/isolated defects within the two functionals.

4.3. Equilibrium Defect Chemistry. As PBE and HSE give similar reaction enthalpies, they would predict comparable

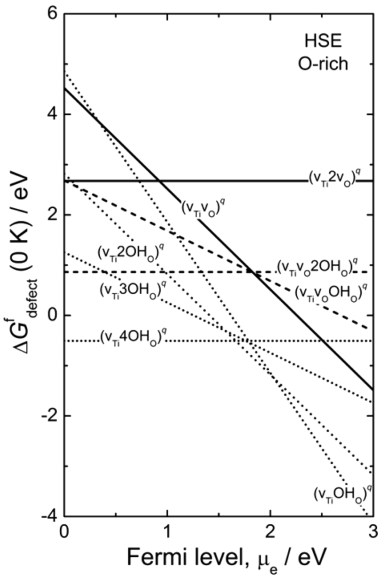

Figure 6. Formation energies of selected complex defects in rutile TiO_2 under oxygen-rich conditions at 0 K obtained with the HSE functional.

Table 3. Binding Enthalpies (in eV) of Included Association Complexes As Obtained with PBE, +U, and HSE

	PBE	+U	HSE
$(v_{Ti}v_O)^{//}$	−1.26	−1.56	−1.23
$(v_{Ti}2v_O)^{\times}$	−1.80	−2.82	−1.88
$(v_{Ti}OH_O)^{3/}$	−0.57	−0.75	−0.58
$(v_{Ti}2OH_O)^{//}$	−0.94	−1.73	−1.10
$(v_{Ti}3OH_O)^{/}$	−1.02	−2.36	−1.14
$(v_{Ti}4OH_O)^{\times}$	−1.13	−2.82	−1.39
$(v_{Ti}v_OOH_O)^{/}$	−1.50	−2.27	−1.36
$(v_{Ti}v_O2OH_O)^{\times}$	−1.67	−2.92	−1.47

equilibrium concentrations of the ionic defects when applying the electroneutrality condition (eq 13). However, underestimation of the band gap in PBE results in errors in the equilibrium Fermi level and thus also in the concentrations of electronic defects. Hence, the following results and discussions are based on the HSE results.

Undoped Rutile TiO_2. The thermal equilibrium formation energies and corresponding concentrations of all included defects (i.e., assuming the entire crystal may reach equilibrium at each temperature/atmospheric condition) are obtained by solving the complete electroneutrality condition

$$\begin{aligned} &4[v_{Ti}^{4/}] + 3[(v_{Ti}OH_O)^{3/}] + 2[(v_{Ti}2OH_O)^{//}] \\ &\quad + [(v_{Ti}3OH_O)^{/}] + 2[(v_{Ti}v_O)^{//}] \\ &\quad + [(v_{Ti}v_OOH_O)^{/}] + 2[(O_2)_O^{//}] + [(O_2)_O^{/}] \\ &\quad + n = 4[Ti_i^{4\bullet}] + 3[Ti_i^{3\bullet}] + 2[v_O^{\bullet\bullet}] + [OH_O^{\bullet}] \\ &\qquad + [H_O^{\bullet}] + p \end{aligned} \tag{23}$$

Figure 7 displays the defect concentrations in undoped TiO_2 under wet, oxidizing conditions (p_{O_2} = 1 atm atm and p_{H_2O} =

dx.doi.org/10.1021/jp304146e | J. Phys. Chem. C 2013, 117, 5919−5930

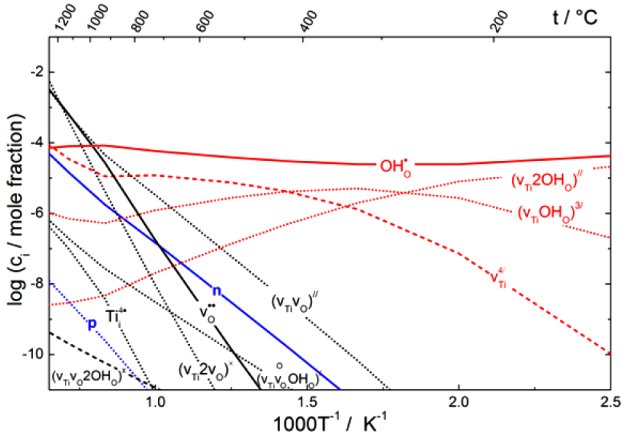

Figure 7. Equilibrium defect concentrations in bulk, undoped TiO_2 as a function of inverse temperature at p_{O_2} = 1 atm and p_{H_2O} = 0.025 atm.

0.025 atm) as a function of inverse temperature. The material displays three distinct defect regimes under these conditions.

At low temperatures (up to ∼300 °C), the material is completely dominated by protonic defects, $OH_O^•$, which are charge compensated by partially hydrated Ti-vacancies, $(v_{Ti}nOH_O)^{(4-n)/}$, or

$$2[(v_{Ti}2OH_O)^{//}] + 3[(v_{Ti}OH_O)^{3/}] = [OH_O^•] \quad (24)$$

At increasing temperatures, the $(v_{Ti}nOH_O)^{(4-n)/}$ complexes dehydrate and are replaced by the unhydrated Ti vacancy. Hence, in the mid-temperature regime (∼300−1000 °C), the dominating electroneutrality is

$$4[v_{Ti}^{4/}] = [OH_O^•] \quad (25)$$

and the material thus hydrates according to eq 4.

At temperatures above ∼900 °C, the concentration of protons decreases and they are replaced by $v_O^{••}$ as the dominating positive defect, which again are charge compensated by $v_{Ti}^{4/}$ and the material is dominated by Schottky disorder. Further, the concentration of the complexes between the two vacancies increases with increasing temperature and the electroneutrality will at the highest temperatures be dominated by

$$4[v_{Ti}^{4/}] + 2[(v_{Ti}v_O)^{//}] = 2[v_O^{••}] \quad (26)$$

while the effectively neutral $(v_{Ti}2v_O)^×$ dominates concentration-wise at the highest temperatures. Finally, these calculations predict an n-type behavior within the entire temperature interval.

Figure 8 displays the defect concentrations in undoped TiO_2 as a function of p_{H_2O} under oxidizing conditions (a) and p_{O_2} under wet conditions (b) at 1000 K. At this temperature, TiO_2 displays the electroneutrality in eq 25 and is thus hydrated according to eq 4 under oxidizing conditions. Upon decreasing p_{H_2O}, the concentration of $OH_O^•$ and $v_{Ti}^{4/}$ decreases according to eq 4, and they are replaced by $v_O^{••}$ and $(v_{Ti}v_O)^{//}$ under the driest conditions. Further, under wet conditions, n increases with decreasing p_{O_2} according to $p_{O_2}^{-1/4}$ (see Figure 8b), and finally surpasses the concentration of the negative $v_{Ti}^{4/}$ related defects at the lowest p_{O_2}, resulting in the situation:

$$n = [OH_O^•] \propto p_{O_2}^{-1/8} \quad (27)$$

Hence, TiO_2 will under such conditions dissolve protons through compensation by electrons according to eq 3. Although we did

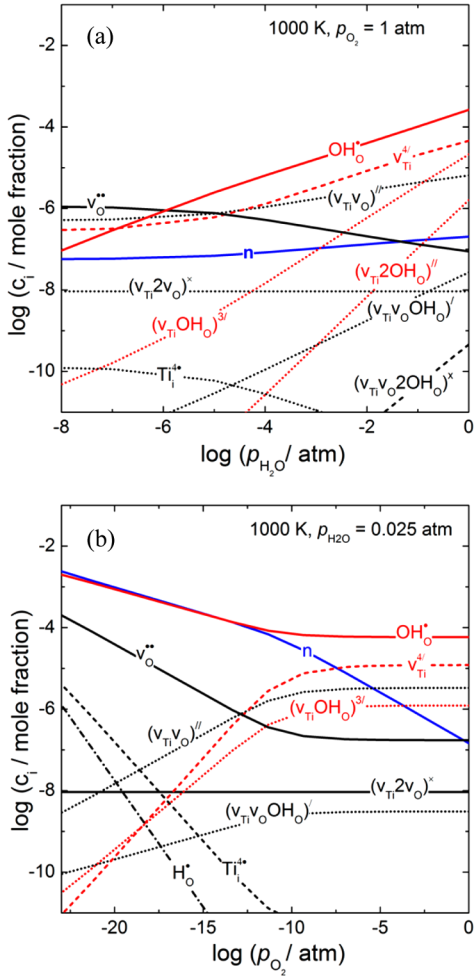

Figure 8. Thermal equilibrium defect concentrations in undoped TiO_2 as a function of (a) p_{H_2O} with p_{O_2} = 1 atm and (b) p_{O_2} with p_{H_2O} = 0.025 atm at 1000 K.

not observe any indications of such equilibria in our experimental work on acceptor doped TiO_2,[10] this situation has been shown to dominate in for instance ZnO under reducing conditions at higher temperatures.[56−58] At higher temperatures and under drier conditions where protons are more unstable, the results predict $2[v_O^{••}] = n \propto p_{O_2}^{-1/6}$ to dominate, which is the situation observed experimentally at low p_{O_2}.[3]

Under all explored p_{H_2O}, p_{O_2}, and temperatures, the calculations predict the complexes $(v_{Ti}v_OOH_O)^/$ and $(v_{Ti}v_O2OH_O)^×$ to be in complete minority. Further, both $Ti_i^{4•}$ and $H_O^•$ are in minority with respect to $v_O^{••}$ and $OH_O^•$. However, at the very highest temperatures, the concentration ratio of $Ti_i^{4•}$ to $v_O^{••}$ decreases due to the more pronounced temperature dependency of $[Ti_i^{4•}]$. Although $Ti_i^{3•}$ have been indicated experimentally,[3] our results predict these to be in minority with respect to $Ti_i^{4•}$ due to their shallow transition level, and we have thus omitted $[Ti_i^{3•}]$ in the following discussions. However, under conditions where the Fermi level is pinned close to the conduction band (i.e., strongly reducing conditions) the concentration of $Ti_i^{3•}$ would approach that of $Ti_i^{4•}$. Finally, the concentrations of $(O_2)_O^q$ (q = 0, −1, and −2) are minute compared the remaining defects under all conditions, and are below the range used in Figures 7 and 8.

dx.doi.org/10.1021/jp304146e | J. Phys. Chem. C 2013, 117, 5919−5930

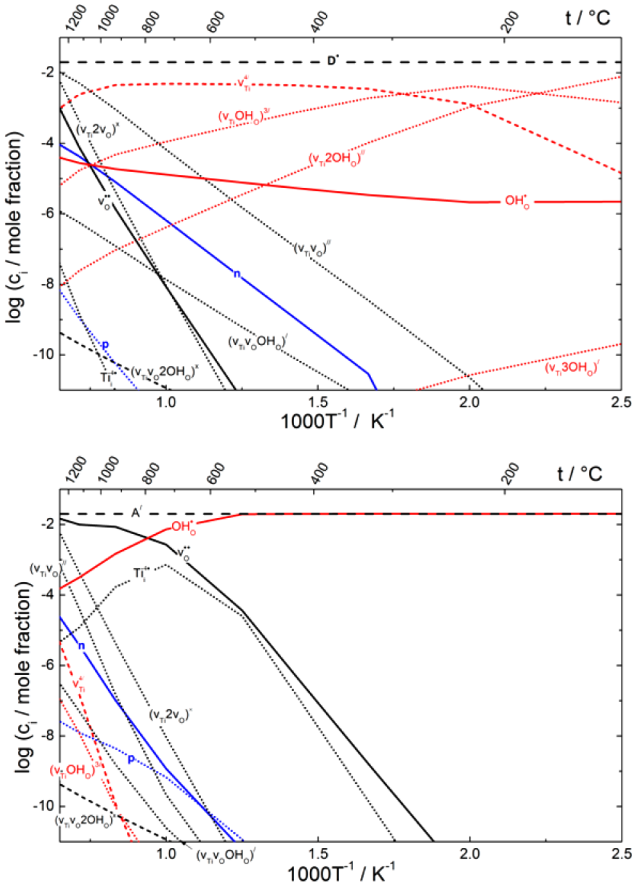

Figure 9. Calculated thermal equilibrium defect concentrations as a function of inverse temperature for 0.02 mole fraction donor and acceptor doped TiO_2 at p_{O_2} = 1 atm, p_{H_2O} = 0.025 atm, and 1000 K.

Aliovalent Doped Rutile TiO_2. Figure 9 displays the concentration of all defects in 0.02 mole fraction donor and acceptor doped rutile TiO_2 as a function of inverse temperature, while Figure 10 displays the corresponding p_{O_2} (left) and p_{H_2O} (right) dependencies at 1000 K. Due to the low equilibrium defect concentrations in undoped TiO_2 (Figures 7 and 8), the dopants affect the defect structure significantly, especially at low to moderate temperatures. Donor doping suppresses the concentration of the dominating positive defects, $v_O^{\bullet\bullet}$ and $OH_O^{\bullet}$, and the frozen-in donor takes over as the dominating positive charge compensating defect. At low and moderate temperatures, donor doped TiO_2 thus displays

$$2[(v_{Ti}2OH_O)^{//}] + 3[(v_{Ti}OH_O)^{3/}] = [D^{\bullet}] \quad (28)$$

while

$$4[v_{Ti}^{4/}] = [D^{\bullet}] \quad (29)$$

dominates at somewhat higher temperatures. From the p_{H_2O} dependency (Figure 10), hydration of donor doped TiO_2 may be described as hydration of the cation vacancies. However, due to the dominating defect situation (eqs 28 and 29) the minority electron concentration, and thus the n-type conductivity, is p_{H_2O} independent. Similarly, eqs 28 and 29 result in a $p_{O_2}^{-1/4}$ dependent minority concentration of electrons, which finally surpasses that of $v_{Ti}^{4/}$ resulting in $n = [D^{\bullet}]$ only at the very lowest p_{O_2} (Figure 10).

Acceptor doping suppresses the concentration of all negative defects, and the aforementioned dominant low temperature defec situation involving the Ruetschi type defects is completely suppressed. As such, the acceptor forms the dominant negative defect and is charge compensated according to

$$[A^{/}] = [OH_O^{\bullet}] + 2[v_O^{\bullet\bullet}] \quad (30)$$

within the entire temperature, p_{O_2} and p_{H_2O} intervall. The concentrations of $v_O^{\bullet\bullet}$, $OH_O^{\bullet}$, and $Ti_i^{4\bullet}$ are under these conditions p_{O_2} independent (Figure 10), and the concentration of $Ti_i^{4\bullet}$ is predicted to be lower than that of oxygen vacancies under all conditions. Hence, hydration of acceptor doped TiO_2 (Figure 10) may be viewed as hydration of oxygen vacancies according to eq 2 under both oxidizing and reducing conditions, as observed experimentally for Fe-doped TiO_2.[10]

Ti Vacancy Doped TiO_2. In the preceding discussion, we assumed that all parts of the crystal could achieve equilibrium with its surroundings at all temperatures. Although this may be the case in near-surface layers or thin films, this does not necessarily apply to bulk specimens. In the following section, we make the assumption that the cation lattice of our system is frozen-in at temperatures below 1500 K, whereas the oxygen lattice may reach equilibrium within the entire temperature range considered. Hence, below this temperature, the total concentration of all defects within the cation lattice remains constant and equal to a total lattice cation vacancy concentration (c_v)

$$\sum_{n=1}^{4} [(v_{Ti}nOH_O)^{(4-n)/}] + [(v_{Ti}2v_O)^{\times}] + [(v_{Ti}v_O)^{//}] + [v_{Ti}^{4/}] = c_v \quad (31)$$

The electroneutrality (eq 23) still applies, and defects within the oxygen lattice and $Ti_i^{4\bullet}$ are assumed formed according to their formation energies as before. The concentrations of the different complexes are described through association of the isolated, mobile oxygen lattice defects with the immobile cation lattice defects, for instance

$$v_{Ti}^{4/} + v_O^{\bullet\bullet} = (v_{Ti}v_O)^{//} \rightarrow \frac{[(v_{Ti}v_O)^{//}]}{[v_{Ti}^{4/}][v_O^{\bullet\bullet}]} = c_{s,r}N_{c,r}\exp\left(-\frac{\Delta H^{b}_{(v_{Ti}v_O)^{//}}}{k_bT}\right) \quad (32)$$

where $c_{s,r}$ is the relative number of defect sites and $N_{c,r}$ the relative number configurations per site for the defects involved in the association reaction and $\Delta H^{b}_{(v_{Ti}v_O)^{//}}$ is the binding enthalpy of the complex as listed in Table 3. Combination of eqs 31 and 32 with eq 23 and the formation energies of the remaining isolated defects (eq 5) thus yields the concentration of all included defects as before.

The resulting defect concentrations, assuming c_v = 0.02 mole fraction, are plotted as a function of inverse temperature in Figure 11. Compared to the thermal equilibrium case for undoped TiO_2 (Figure 7), all defect concentrations appear higher due to the effective acceptor doping of the material by the immobile cation defects. Further, the concentrations of the Ruetschi type defects are greatly promoted, and the material is dominated primarily by

$$2[(v_{Ti}2OH_O)^{//}] = [OH_O^{\bullet}] \quad (33)$$

dx.doi.org/10.1021/jp304146e | J. Phys. Chem. C 2013, 117, 5919−5930

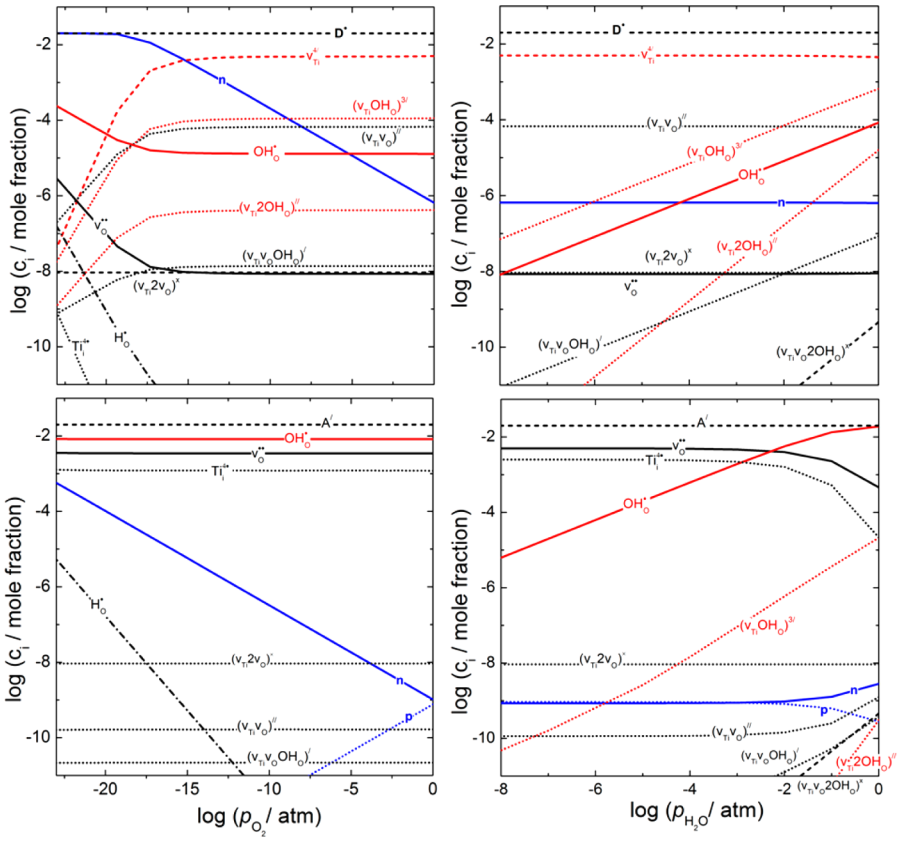

Figure 10. Equilibrium defect concentrations in 0.02 mole fraction donor or acceptor doped TiO_2 versus (left) p_{O_2} (at p_{H_2O} = 0.025 atm) and (right) p_{H_2O} (at p_{O_2} = 1 atm) at 1000 K.

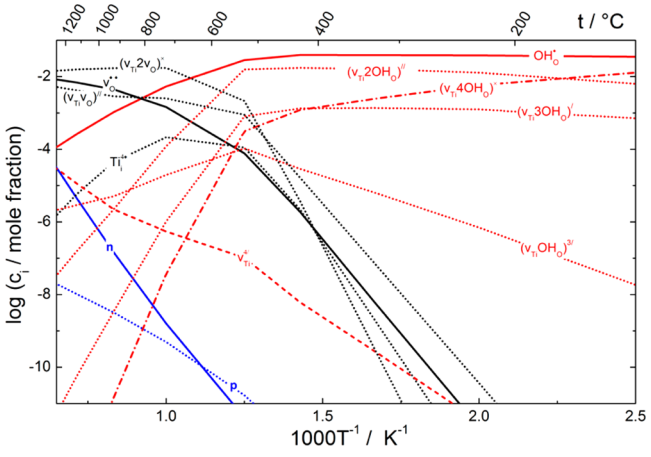

Figure 11. Defect concentrations as a function of inverse temperature under wet, oxidizing conditions (p_{O_2} = 1 atm and p_{H_2O} = 0.025 atm) when assuming an immobile cation lattice. The minority complexes $(v_{Ti}v_O OH_O)^{/}$ and $(v_{Ti}v_O 2OH_O)^{\times}$ are omitted for clarity.

at temperatures up to around 600−700 °C. Under drier conditions, the cation vacancies would be compensated by $v_O^{\bullet\bullet}$ and hydration of the cation deficient material may therefore be described by eq 2 and simultaneous hydration of the frozen-in cation vacancies (without increasing the total cation vacancy concentration). At higher temperatures, the Schottky-like complexes dominate, and protons are replaced by oxygen vacancies as the dominating positive defect

$$[(v_{Ti}v_O)^{//}] = [v_O^{\bullet\bullet}] \quad (34)$$

The concentration of both Schottky-like complexes increases with increasing temperature due to the increasing concentration of $v_O^{\bullet\bullet}$ (see eq 32). However, they level off and eventually decrease at the very the highest temperatures, yielding a Schottky dominated situation with dissociated complexes.

Further, under humid conditions, vacancy doped TiO_2 is predicted to be p-type at lower and n-type at higher temperatures. However, n and p are in both regions highly p_{H_2O} dependent, and the material could thus be effectively p-type doped by freezing in cation vacancies followed by dehydration at moderate temperatures. Finally, an interesting effect of vacancy doping is the increased concentration of protons at lower temperatures (Figure 11) compared to both the undoped, acceptor, and donor doped TiO_2 (Figures 7 and 9).

4.4. Experimental Signatures. In the preceding sections, we showed that the defect structure of TiO_2 at lower temperatures is dominated by cation vacancies, protonic defects and their mutual association complexes. As the structural environment (for instance O−H and OH..O bonds) are affected by the trapping of H in the various vacancy complexes compared to the nonassociated $OH_O^{\bullet}$ defect (see Figures 4 and 5), one would also expect changes in the characteristic vibrational properties of H in the different environments.

Table 4 lists the calculated frequencies of the O−H stretch modes of the $OH_O^{\bullet}$, $(v_{Ti}OH_O)^{3/}$ (with H in configuration H_a) and $(v_{Ti}4OH_O)^{\times}$ (with two antiparallel H_a and two antiparallel H_b) defects as obtained from finite displacement phonon calculation (using PBE). The higher wavenumber of the O−H stretch mode of the $(v_{Ti}OH_O)^{3/}$ complex compared to $OH_O^{\bullet}$ indicates a stronger O−H bond in the former, reflected also by the shorter

dx.doi.org/10.1021/jp304146e | J. Phys. Chem. C 2013, 117, 5919−5930

Table 4. Wave Numbers of the O−H Stretch Modes of Different H-Containing Defects As Obtained with Finite Displacement Phonon Calculations Using PBE

defect	ν/cm^{-1}
$OH_O^{\bullet}$	3423
$(v_{Ti}OH_O)^{3/}$	3596
$(v_{Ti}4OH_O)^{\times}$	3524/3524/3321/3321

O−H bond length in $(v_{Ti}OH_O)^{3/}$ than $OH_O^{\bullet}$. Further, addition of three additional protons in the vacancy (i.e., addition of one H_a and two H_b) results in two 2-fold degenerate modes; with higher and lower wave numbers than that of $OH_O^{\bullet}$, respectively. The slight lowering of the highest modes in the $(v_{Ti}4OH_O)^{\times}$ complex (i.e., those corresponding to the two H_a) compared to $(v_{Ti}OH_O)^{3/}$ reflects a slight destabilization of the protons due to their mutual repulsion, as also reflected by the lower binding enthalpy per proton of $(v_{Ti}4OH_O)^{\times}$ than $(v_{Ti}OH_O)^{3/}$. However, by thermodynamic modeling, we indicated that the low temperature defect chemistry of TiO_2 will be dominated by $OH_O^{\bullet}$, $(v_{Ti}OH_O)^{3/}$, and $(v_{Ti}2OH_O)^{//}$, which thus determine the vibrational properties of the material. Hence, one would expect an experimental IR spectrum of hydrated, cation defective TiO_2 to exhibit a splitting of the characteristic O−H peaks, which thus would support the theoretical findings outlined in this work.

5. SUMMARY

This work describes the defect chemistry of bulk rutile TiO_2 through first principles DFT based defect calculations employing various exchange-correlation functionals. We have included the most common isolated point defects, and their mutual complexes. The formation energies of the complexes between $v_{Ti}^{4/}$, $v_O^{\bullet\bullet}$, and $OH_O^{\bullet}$ are as low, or even lower than those of the isolated defects, and all included complexes display exothermic binding enthalpies, and such defects should therefore be accounted for in the evaluation of the materials' defect structure. Extrapolation of DFT obtained formation energies to finite temperatures reveals that the defect chemistry of undoped rutile TiO_2 largely is dominated by $v_{Ti}^{4/}$, $OH_O^{\bullet}$ and their mutual complexes under oxidizing conditions and lower temperatures, and by $v_{Ti}^{4/}$, $v_O^{\bullet\bullet}$, and their complexes at higher temperatures. The results show that the defect chemistry of TiO_2 cooled from high temperatures or grown at low temperatures (for instance as oxide scales on metals or as nanodimensional films or other morphologies), will have defect structures very different from previously known. Together with our previous results for defects in surfaces,[59] this gives a new basis for understanding photocatalytic properties of TiO_2. Obviously, similar studies should follow for anatase TiO_2 as for rutile TiO_2 here.

AUTHOR INFORMATION

Corresponding Author

*E-mail: truls.norby@kjemi.uio.no.

Notes

The authors declare no competing financial interest.

ACKNOWLEDGMENTS

The authors gratefully acknowledge the Norwegian metacenter for computational science for proving computational resources under Project No. NN4604k.

REFERENCES

(1) Fujishima, A.; Honda, K. Electrochemical Photolysis of Water at a Semiconductor Electrode. *Nature* **1972**, *238* (5358), 37−38.
(2) Nowotny, M. K.; Sheppard, L. R.; Bak, T.; Nowotny, J. Defect Chemistry of Titanium Dioxide. Application of Defect Engineering in Processing of TiO_2-Based Photocatalysts. *J. Phys. Chem. C* **2008**, *112*, 5275−5300.
(3) Nowotny, J.; Bak, T.; Nowotny, M. K.; Sheppard, L. R. Defect Chemistry and Electrical Properties of Titanium Dioxide. 2. Effect of Aliovalent Ions. *J. Phys. Chem. C* **2008**, *112* (2), 602−610.
(4) Cronemeyer, D. C. Infrared Absorption of Reduced Rutile TiO_2 Single Crystals. *Phys. Rev.* **1959**, *113* (5), 1222−1226.
(5) Johnson, O. W.; Paek, S. H.; DeFord, J. W. Diffusion of H and D in TiO_2: Suppression of internal fields by isotope exchange. *J. Appl. Phys.* **1975**, *46* (3), 1026−1033.
(6) Bates, J. B.; Perkins, R. A. Infrared Spectral Properties of Hydrogen, Deuterium, and Tritium in TiO_2. *Phys. Rev. B* **1977**, *16* (8), 3713−3722.
(7) Cathcart, J. V.; Perkins, R. A.; Bates, J. B.; Manley, L. C. Tritium diffusion in rutile (TiO_2). *J. Appl. Phys.* **1979**, *50* (6), 4110−4119.
(8) Bates, J. B.; Wang, J. C.; Perkins, R. A. Mechanisms for Hydrogen Diffusion in TiO_2. *Phys. Rev. B* **1979**, *19* (8), 4130.
(9) Bjørheim, T. S.; Stølen, S.; Norby, T. Ab Initio Studies of Hydrogen and Acceptor Defects in Rutile TiO_2. *Phys. Chem. Chem. Phys.* **2010**, *12* (25), 6817−6825.
(10) Erdal, S.; Kongshaug, C.; Bjørheim, T. S.; Jalarvo, N.; Haugsrud, R.; Norby, T. Hydration of Rutile TiO_2: Thermodynamics and Effects on n- and p-Type Electronic Conduction. *J. Phys. Chem. C* **2010**, *114* (19), 9139−9145.
(11) Koudriachova, M. V.; de Leeuw, S. W.; Harrison, N. M. First-Principles Study of H Intercalation in Rutile TiO_2. *Phys. Rev. B* **2004**, *70* (16), 165421.
(12) Nowotny, J.; Norby, T.; Bak, T. Reactivity Between Titanium Dioxide and Water at Elevated Temperatures. *J. Phys. Chem. C* **2010**, *114* (42), 18215−18221.
(13) Nowotny, J. Effect of Hydrogen on Semiconducting Properties of TiO_2 Single Crystal Jonker Analysis. *J. Phys. Chem. C* **2011**, *115* (37), 18316−18326.
(14) Weber, J.; Lavrov, E. V.; Herklotz, F. Hydrogen Shallow Donors in ZnO and Rutile TiO_2. *Physica B* **2012**, *407* (10), 1456−1461.
(15) Balachandran, D.; Morgan, D.; Ceder, G.; van de Walle, A. First-Principles Study of the Structure of Stoichiometric and Mn-Deficient MnO_2. *J. Solid State Chem.* **2003**, *173* (2), 462−475.
(16) Grey, I. E.; Wilson, N. C. Titanium Vacancy Defects in Sol-Gel Prepared Anatase. *J. Solid State Chem.* **2007**, *180* (2), 670−678.
(17) Varley, J. B.; Peelaers, H.; Janotti, A.; Van de Walle, C. G. Hydrogenated Cation Vacancies in Semiconducting Oxides. *J. Phys.: Condens. Matter* **2011**, *23* (33), 334212.
(18) Thomas, A. G.; Flavell, W. R.; Mallick, A. K.; Kumarasinghe, A. R.; Tsoutsou, D.; Khan, N.; Chatwin, C.; Rayner, S.; Smith, G. C.; Stockbauer, R. L.; et al. Comparison of the Electronic Structure of Anatase and Rutile TiO_2 Single-Crystal Surfaces Using Resonant Photoemission and X-Ray Absorption Spectroscopy. *Phys. Rev. B* **2007**, *75* (3), 035105.
(19) Zhang, Z.; Jeng, S.-P.; Henrich, V. E. Cation-Ligand Hybridization for Stoichiometric and Reduced TiO_2 (110) Surfaces Determined by Resonant Photoemission. *Phys. Rev. B* **1991**, *43* (14), 12004−12011.
(20) Nerlov, J.; Ge, Q.; Møller, P. J. Resonant Photoemission from TiO_2 (110) Surfaces: Implications on Surface Bonding and Hybridization. *Surf. Sci.* **1996**, *348* (1−2), 28−38.
(21) Zhou, S.; Čižmár, E.; Potzger, K.; Krause, M.; Talut, G.; Helm, M.; Fassbender, J.; Zvyagin, S. A.; Wosnitza, J.; Schmidt, H. Origin of Magnetic Moments in Defective TiO_2 Single Crystals. *Phys. Rev. B* **2009**, *79* (11), 113201.
(22) Yang, S.; Halliburton, L. E.; Manivannan, A.; Bunton, P. H.; Baker, D. B.; Klemm, M.; Horn, S.; Fujishima, A. Photoinduced Electron Paramagnetic Resonance Study of Electron Traps in TiO_2 Crystals: Oxygen Vacancies and Ti^{3+} ions. *Appl. Phys. Lett.* **2009**, *94* (16), 162114−3.

(23) Diebold, U. The Surface Science of Titanium Dioxide. *Surf. Sci. Rep.* **2003**, *48* (5−8), 53−229.
(24) Di Valentin, C.; Pacchioni, G.; Selloni, A. Electronic structure of defect states in hydroxylated and reduced rutile TiO_2 (110) surfaces. *Phys. Rev. Lett.* **2006**, *97* (16), 166803.
(25) Morgan, B. J.; Watson, G. W. A DFT + U Description of Oxygen Vacancies at the TiO_2 Rutile (110) Surface. *Surf. Sci.* **2007**, *601* (21), 5034−5041.
(26) Morgan, B. J.; Watson, G. W. A Density Functional Theory + U Study of Oxygen Vacancy Formation at the (110), (100), (101), and (001) Surfaces of Rutile TiO_2. *J. Phys. Chem. C* **2009**, *113* (17), 7322−7328.
(27) Morgan, B. J.; Watson, G. W. Polaronic Trapping of Electrons and Holes by Native Defects in Anatase TiO_2. *Phys. Rev. B* **2009**, *80* (23), 233102.
(28) Morgan, B. J.; Watson, G. W. Intrinsic n-type Defect Formation in TiO_2: A Comparison of Eutile and Anatase from GGA+U Calculations. *J. Phys. Chem. C* **2010**, *114* (5), 2321−2328.
(29) Bonapasta, A. A.; Filippone, F.; Mattioli, G.; Alippi, P. Oxygen vacancies and OH species in rutile and anatase TiO_2 polymorphs. *Catal. Today* **2009**, *144* (1−2), 177−182.
(30) Stausholm-Møller, J.; Kristoffersen, H. H.; Hinnemann, B.; Madsen, G. K. H.; Hammer, B. DFT+U Study of Defects in Bulk Rutile TiO_2. *J. Chem. Phys.* **2010**, *133* (14), 144708−8.
(31) Janotti, A.; Varley, J. B.; Rinke, P.; Umezawa, N.; Kresse, G.; Van de Walle, C. G. Hybrid Functional Studies of the Oxygen Vacancy in TiO_2. *Phys. Rev. B* **2010**, *81* (8), 085212.
(32) von Oertzen, G. U.; Gerson, A. R. The Effects of O Deficiency on the Electronic Structure of Rutile TiO_2. *J. Phys. Chem. Solids* **2007**, *68* (3), 324−330.
(33) Mattioli, G.; Filippone, F.; Alippi, P.; Amore Bonapasta, A. Ab Initio Study of the Electronic States Induced by Oxygen Vacancies in Rutile and Anatase TiO_2. *Phys. Rev. B* **2008**, *78* (24), 241201.
(34) Filippone, F.; Mattioli, G.; Alippi, P.; Amore Bonapasta, A. Properties of Hydrogen and Hydrogen-Vacancy Complexes in the Rutile Phase of Titanium Dioxide. *Phys. Rev. B* **2009**, *80* (24), 245203.
(35) Finazzi, E.; Di Valentin, C.; Pacchioni, G. Nature of Ti Interstitials in Reduced Bulk Anatase and Rutile TiO_2. *J. Phys. Chem. C* **2009**, *113* (9), 3382−3385.
(36) Deák, P.; Aradi, B.; Frauenheim, T. Polaronic effects in TiO_2 calculated by the HSE06 hybrid functional: Dopant passivation by carrier self-trapping. *Phys. Rev. B* **2011**, *83* (15), 155207.
(37) Peng, H. First-principles study of native defects in rutile TiO_2. *Phys. Lett. A* **2008**, *372* (9), 1527−1530.
(38) He, J.; Behera, R. K.; Finnis, M. W.; Li, X.; Dickey, E. C.; Phillpot, S. R.; Sinnott, S. B. Prediction of High-Temperature Point Defect Formation in TiO_2 from Combined Ab Initio and Thermodynamic Calculations. *Acta Mater.* **2007**, *55* (13), 4325−4337.
(39) Li, X.; Finnis, M. W.; He, J.; Behera, R. K.; Phillpot, S. R.; Sinnott, S. B.; Dickey, E. C. Energetics of Charged Point Defects in Rutile TiO_2 By Density Functional Theory. *Acta Mater.* **2009**, *57* (19), 5882−5891.
(40) Mattioli, G.; Alippi, P.; Filippone, F.; Caminiti, R.; Amore Bonapasta, A. Deep Versus Shallow Behavior of Intrinsic Defects in Rutile and Anatase TiO_2 Polymorphs. *J. Phys. Chem. C* **2010**, *114* (49), 21694−21704.
(41) Park, S.-G.; Magyari-Köpe, B.; Nishi, Y. Electronic Correlation Effects in Reduced Rutile TiO_2 Within the LDA+U Method. *Phys. Rev. B* **2010**, *82* (11), 115109.
(42) Kresse, G.; Furthmüller, J. Efficient Iterative Schemes for Ab Initio Total-Energy Calculations Using a Plane-Wave Basis Set. *Phys. Rev. B* **1996**, *54* (16), 11169.
(43) Kresse, G.; Joubert, D. From Ultrasoft Pseudopotentials to the Projector Augmented-Wave Method. *Phys. Rev. B* **1999**, *59* (3), 1758.
(44) Perdew, J. P.; Burke, K.; Ernzerhof, M. Generalized Gradient Approximation Made Simple. *Phys. Rev. Lett.* **1996**, *77* (18), 3865.
(45) Heyd, J.; Scuseria, G. E.; Ernzerhof, M. Hybrid Functionals Based on a Screened Coulomb Potential. *J. Chem. Phys.* **2003**, *118* (18), 8207−8215.
(46) Heyd, J.; Scuseria, G. E.; Ernzerhof, M. Erratum: "Hybrid Functionals Based on a Screened Coulomb Potential". *J. Chem. Phys.* **2006**, *124* (21), 219906.
(47) Bocquet, A. E.; Mizokawa, T.; Morikawa, K.; Fujimori, A.; Barman, S. R.; Maiti, K.; Sarma, D. D.; Tokura, Y.; Onoda, M. Electronic Structure of Early 3d-Transition-Metal Oxides by Analysis of the 2p Core-level Photoemission Spectra. *Phys. Rev. B* **1996**, *53* (3), 1161−1170.
(48) Blöchl, P. E. Projector Augmented-wave method. *Phys. Rev. B* **1994**, *50* (24), 17953.
(49) Howard, C. J.; Sabine, T. M.; Dickson, F. Structural and Thermal Parameters for Rutile and Anatase. *Acta Crystallogr. Sect. B* **1991**, *47* (4), 462−468.
(50) Chase, M. W., Jr. *NIST-JANAF Thermochemical Tables*, 4 ed.; The American Institute of Physics for The National Institute of Standards and Technology: New York, 1998.
(51) Pascual, J.; Camassel, J.; Mathieu, H. Fine Structure in the Intrinsic Absorption Edge of TiO_2. *Phys. Rev. B* **1978**, *18* (10), 5606−5614.
(52) Mattila, T.; Zunger, A. Deep Electronic Gap Levels Induced by Isovalent P and As Impurities in GaN. *Phys. Rev. B* **1998**, *58* (3), 1367.
(53) Björketun, M. E.; Sundell, P. G.; Wahnström, G. Structure and Thermodynamic Stability of Hydrogen Interstitials in $BaZrO_3$ Perovskite Oxide from Density Functional Calculations. *Faraday Discuss.* **2007**, *134*, 247−265.
(54) Kamisaka, H.; Yamashita, K. Theoretical Study of the Interstitial Oxygen Atom in Anatase and Rutile TiO_2: Electron Trapping and Elongation of the r(O−O) Bond. *J. Phys. Chem. C* **2011**, *115* (16), 8265−8273.
(55) Lee, H.-Y.; Clark, S. J.; Robertson, J. Calculation of Point Defects in Rutile TiO_2 By the Screened-Exchange Hybrid Functional. *Phys. Rev. B* **2012**, *86* (7), 075209.
(56) Thomas, D. G.; Lander, J. J. Hydrogen as a Donor in Zinc Oxide. *J. Chem. Phys.* **1956**, *25* (6), 1136−1142.
(57) Erdal, S.; Kjølseth, C.; Norby, T. Concentration and Mobility of Electrons in ZnO from Electrical Conductivity and Thermoelectric Power in H_2 + H_2O at High Temperatures. *J. Phys. Chem. C* **2010**, *114* (39), 16785−16792.
(58) Bjørheim, T. S.; Erdal, S.; Johansen, K. M.; Knutsen, K. E.; Norby, T. H and Li Related Defects in ZnO and Their Effect on Electrical Properties. *J. Phys. Chem. C* **2012**, *116* (44), 23764−23772.
(59) Bjørheim, T. S.; Kuwabara, A.; Mohn, C. E.; Norby, T. Defects at the (110) Surface of Rutile TiO_2 from Ab Initio Calculations. *Int. J. Hydrogen Energy* **2012**, *37* (9), 8110−8117.